

The role of the density profile location on pedestal stability in ASDEX Upgrade

M. G. Dunne¹, L. Frassinetti², M. Bernert¹, S. Potzel¹, F. Reimold³, E. Viezzer¹, M. Wischmeier¹, E. Wolfrum¹, M. Bernert¹, M.N.A. Beurskens⁴, M. Cavedon^{1,5}, E. Fable¹, R. Fischer¹, B. Kurzan¹, F. M. Laggner⁶, R. M. McDermott¹, G. Tardini¹, M. Willensdorfer¹, the EUROfusion MST1 Team⁷, and the ASDEX-Upgrade Team¹

¹Max-Planck-Institut für Plasmaphysik, D-85748 Garching, Germany

²Division of Fusion Plasma Physics, KTH Royal Institute of Technology, Stockholm SE

³Forschungszentrum Jülich, D-52425 Jülich, Germany

⁴Max-Planck-Institut für Plasmaphysik, D-17491 Greifswald, Germany

⁵Physik-Department E28, Technische Universität München, Garching Germany

⁶Institute of Applied Physics, TU Wien, Fusion@ÖAW, 1040 Vienna, Austria

⁷ See <http://www.euro-fusionscipub.org/mst1>

E-mail contact of the main author: mike.dunne@ipp.mpg.de

Abstract

The impact of a localised region of high density in the high field side scrape off layer (the high-field side high density, HFSHD), on pedestal structure and stability is presented. Notably, once the HFSHD is formed by a combination of high recycling at the inner target and power crossing the separatrix to ionise the recycled neutrals, the fuelling pattern of the pedestal changes. Instead of simply increasing the pedestal top density, the density profile now shifts outwards, as shown in a gas puff scan. This outward shift, which has been observed to be ~ 5 mm in AUG, causes a significant degradation of the pedestal top pressure, typically manifested as a drop in the temperature. Predictive modelling of the pedestal top pressure indicates a drop of 25% in the attainable pedestal top pressure, which compares well with measurements. Mitigation of the HFSHD by the application of impurity seeding is also shown. Both nitrogen and neon reduce the density in the HFSHD by radiating the power required to ionise the neutrals at the HFS divertor entrance. At similar levels of radiated power, similar shifts of the density profile, and, hence, similar changes in the pedestal top pressure and global confinement are observed.

1 Introduction

Understanding how fuelling and seeding impact the global performance is required as devices such as ITER and DEMO will both operate with these actuators in place to tune the heat loads onto the divertor and possibly also to influence ELM behaviour. In particular, it has now been well established that excessive main ion fuelling, routinely applied in metal-walled devices for impurity control, has a detrimental effect on confinement, while impurity seeding, usually of nitrogen, improves confinement. Recent analysis of core and pedestal profiles has shown that changes in the pedestal height with fuelling and seeding drive the changes in global energy confinement [2, 3, 4, 5]. Up until now, the mechanism(s) behind these changes were unknown.

A set of experiments performed over several years on AUG has shed light on this issue. Most of the measurements have focussed on a medium triangularity shape ($\delta_{av} = 0.25$) with an edge

q of 4.0 ($B_T/I_p = 2.5 \text{ T}/1 \text{ MA}$). As shown in figure 1, increasing the main ion fuelling rate (open circles to open squares, $\Gamma_D = 1.0 \rightarrow 2.7 \times 10^{21} \text{ e}^- \text{ s}^{-1}$) can significantly change the pedestal top pressure. Some of this confinement loss with fuelling can be compensated by simply increasing the heating power, but this is a rather weak effect. Instead, puffing a small quantity of nitrogen (up to $\sim 2\%$) into both scenarios can dramatically increase the pedestal top pressure and mitigate the effects of gas puffing. Shown in figure 1 is the pedestal top pressure in the low gas scenario with added nitrogen seeding (green). At the highest heating power, the attainable pedestal top pressure ranges from 12-20 kPa due to the changes in fuelling and seeding.

In addition to nitrogen, neon and argon are often proposed as better alternatives to nitrogen for power radiation in future devices, since they do not react chemically with wall or fuel materials in a reactor, offering a large advantage over elements such as nitrogen. Examining if it is only nitrogen which has a positive impact on confinement, or if this is a general feature of impurity seeding could offer insight into how fuelling and seeding impact performance. Finally, since the divertor compression of neutrals and impurities is predicted to be significantly higher in future devices, understanding how radiation, both its magnitude and location, and impurity content impact performance is a key question in plasma physics at the moment.

This paper will examine a range of AUG discharges with variations in fuelling and the seeding species and seek to provide a rounded physics picture of the main influences on the pedestal. A brief summary of the influences on the pedestal top and the framework within which it can be analysed is given in section 2. Observations of changes to the pedestal structure with fuelling are shown in section 3, and the mitigation of this effect and corresponding pedestal pressure increase are shown in section 4.

2 Influences on the pedestal

Extensive experiments and modelling in recent years have progressed our understanding of what determines the critical pedestal top in Type-I ELMy H-modes. The limitation in ELMing H-modes is the occurrence of an edge localised mode (ELM) crash, which expels particles and energy from the confined plasma into the scrape-off layer (SOL). The present best model to describe the onset of an ELM is the linear peeling-ballooning (PB) theory, which states that a critical pressure gradient and current density are required to trigger an ELM crash. These critical values are dependent on many plasma properties, such as the edge q value and the global beta[6, 7, 8], and also on pedestal properties such as the pedestal width[6].

Since the PB model returns a critical gradient (or height) as a function of the pedestal width, a second constraint is needed. In the well known EPED model[6], this takes the form of a kinetic ballooning mode (KBM) constraint, which is implemented as a constraint on the pedestal width. In the original EPED model the pedestal width scales as $\Delta_{\text{ped}} = c \times \sqrt{\beta_{\text{pol,ped}}}$, where

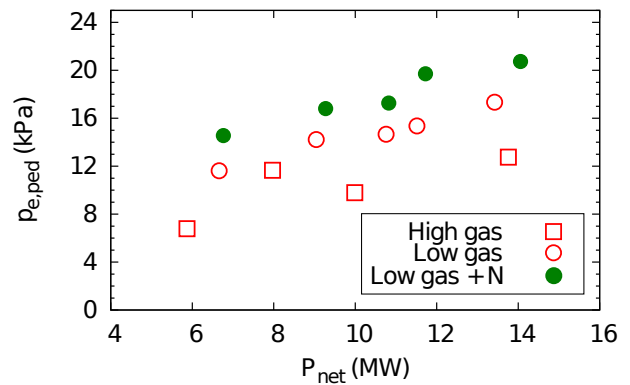


Figure 1: Pedestal top pressure as a function of applied heating power for high gas (red squares), low gas (red circles), and low gas with impurity seeding (filled blue circles).

$\beta_{\text{pol,ped}}$ is the poloidal beta at the pedestal top and c is a constant (typical range between 0.076 and 0.11, taken from fits to DIII-D and AUG data, respectively). In later versions an infinite-n ballooning calculation was used to approximate KBM stability. While advances in pedestal gyrokinetic modelling are being made[9], it is still not a widely used method for determining critical gradients. As a result, and due to the wide range of experimental data showing broad consistency with the $\sqrt{\beta_{\text{pol,ped}}}$ scaling, this will be used in the predictive calculations with the iPED code[5] used in this paper. The iPED code mainly uses the same input parameters as the EPED code (I_p , B_T , plasma shape, pedestal density, global β , Z_{eff}), but also allows the position of the density profile to vary.

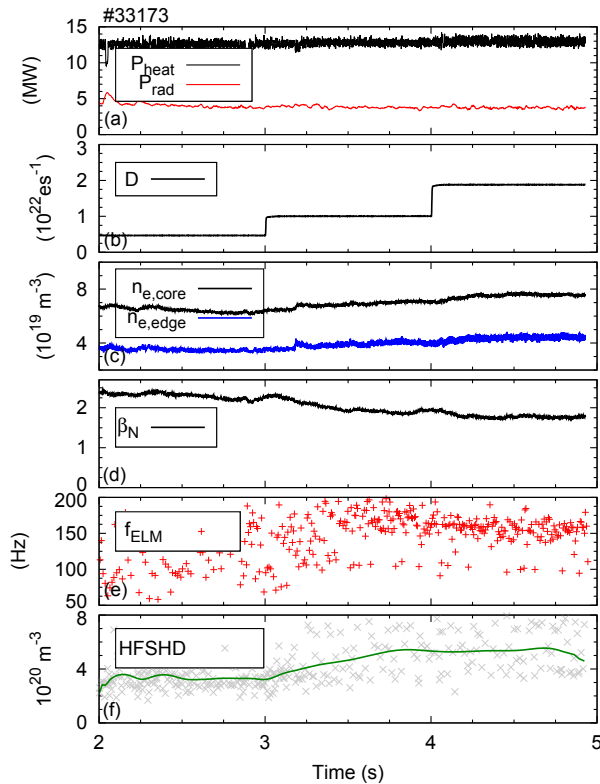


Figure 2: Time traces of (a) heating (black) and radiated (red) power, (b) deuterium fuelling wave form, (c) core (black) and edge (blue) line integrated densities, (d) normalised beta, (e) ELM frequency, and (f) the density in the HFSHD for discharge #33173.

the plasma from neutral penetration dominated to diffusive and drift dominated mechanisms. In particular, the density at the separatrix increases, leading to an effective "outward shift" of the density profile as the magnitude of the density in the HFSHD increases. Small values of this outward shift, or a corresponding inward shift, of $\Delta\rho_{\text{poloidal}} = 0.01$ can change the pedestal top by $\sim 25\%$ [5].

Since the HFSHD is driven by gas fuelling and reduced by radiating input power before it can reach the inner divertor, experiments varying the gas fuelling and impurity seeding with both

This input is allowed in iPED as the position of the density profile has been shown in several devices to have a significant impact on the attainable pedestal top values[10, 11, 5, 12]. Experiments at NSTX[10, 13] showed that a strong reduction in recycling effectively shifts the density profile inwards, while mode excitation in the DIII-D[11] pedestal also did the same. More recently, the discovery of the high field side high density (HFSHD) at AUG[14] has offered a new mechanism to shift the density profile. The HFSHD is a region of high density ($n_{e,\text{HFSHD}} \sim 10 \times n_{e,\text{sep}}$) localised to the HFS SOL, between the divertor and the midplane. The generation mechanism for the HFSHD relies on high recycling conditions near the HFS divertor entrance and power reaching this location to ionise the recycled neutrals[16]. The HFSHD increases with the gas puff and heating power and reduces when the power exhausted from the plasma is radiated before reaching the HFSHD, i.e with impurity seeding.

Since the magnitude of the density in the HFSHD is approximately $10\times$ higher than that at the separatrix, it alters the fuelling of

neon and nitrogen were performed, which will be described in the next sections.

3 Shifting the density profile

For these experiments, a standard AUG scenario was taken ($I_p = 1$ MA, $B_T = -2.5$ T, $\delta = 0.25$, $\kappa = 1.7$, $R_{\text{geo}} = 1.7$, $a_{\text{minor}} = 0.5$). In a single discharge, time traces of which are shown in figure 2, the heating power was kept constant at 10 MW while the gas fuelling rate was increased in three steps from 0.5-1.0- $2.0 \times 10^{-5} \text{ s}^{-1}$. In each of these steps, the density in the HFSHD increased, while the stored energy in the plasma decreased.

A strong increase in the HFSHD can be seen between the first and second fuelling steps in this discharge, which corresponds to the large drop observed in stored energy. Between the second and third steps, a smaller increase in the HFSHD corresponds to a smaller drop in the stored energy. For a comparison of the changes in the pedestal, data from the first and third steps were analysed and are shown in figure 3.

At the higher fuelling level, the temperature pedestal (a) becomes lower and narrower. At the same time, the density pedestal (b) increases and shifts outwards. This outward shift, driven by the change in fuelling caused by the presence of the HFSHD, then causes the attainable pedestal pressure (c) to be reduced. As can clearly be seen, the pressure gradient is now located closer to the separatrix, which means a lower pedestal top pressure can be sustained. This same link between a relative shift of the temperature and density profile and the attainable pedestal top pressure was also recently reported on the JET tokamak [12], though work is still ongoing to examine if it also has its roots in the HFSHD (which has been observed at JET [15] or some other mechanism. An analysis of a power and gas scan showed that the shift between the profile increased with increasing gas and heating power, as would be expected if it were caused by the increased HFSHD.

4 Mitigating the HFSHD

Since the HFSHD can be mitigated by radiating exhaust power before it reaches the HFS divertor, impurity seeding lends itself as an obvious candidate. In the best case scenario, the power

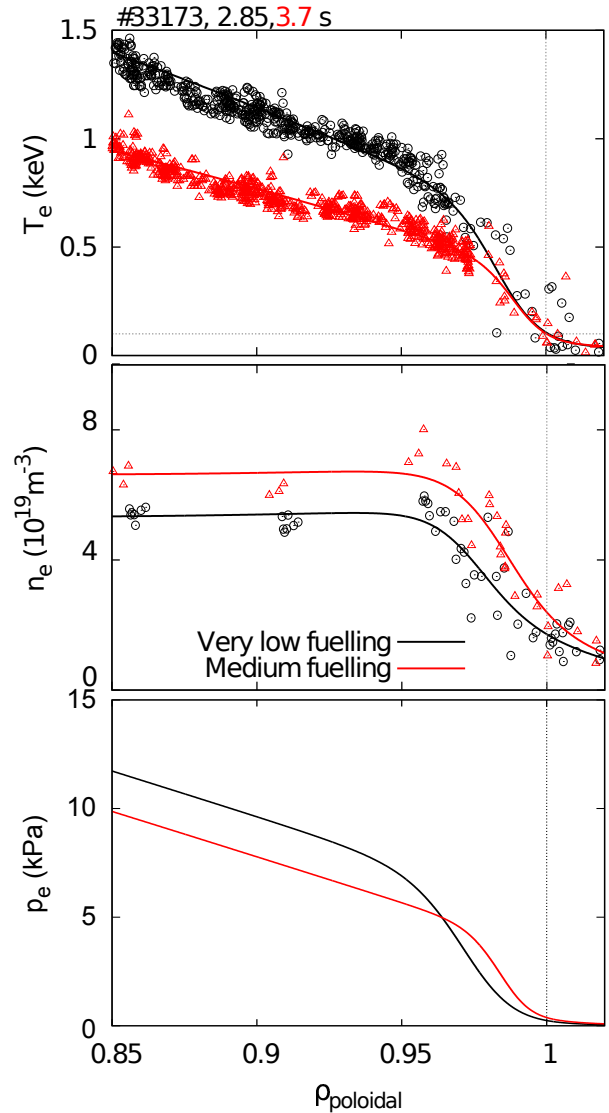


Figure 3: Profiles of (a) electron temperature, (b) electron density, and (c) electron pressure for discharge #33173 during low (black) and high (red) fuelling steps.

would only be radiated outside of the confined plasma, ensuring that H-mode operation remains stable. This implies that nitrogen is a good choice to mitigate the HFSHD. Neon, however, is also a possible option, since it also radiates at low temperatures and has the added advantage of being chemically inert; for these reasons, neon is the radiator of choice for future JET-ILW DT experiments, and also the preferred radiator for ITER. It has been shown many times in recent years that nitrogen seeding has a positive impact on confinement in JET-ILW[4, 17] and AUG[2, 18], and its benefit for the reduction of power to the target plates over gas fuelling alone was also highlighted on C-Mod[19].

This change of confinement with nitrogen seeding was shown to originate in the pedestal[5, 17] and it was also recently demonstrated at AUG that this effect arises from the mitigation of the HFSHD and the subsequent inward shift of the density profile[20]. This inward shift then allows an increase of the pedestal top pressure by $\sim 25\%$, corresponding well to the experimentally observed values.

The hypothesis that the impurity radiation is the dominant drive for reducing the HFSHD implies that medium-Z impurity seeding should all have the same effect, given the same amount of total radiated power. This was shown in AUG[21], comparing low and high triangularity phases of discharges with no seeding, with CD_4 seeding, and with nitrogen seeding. Since carbon and nitrogen are chemically similar, they radiate in similar locations (predominantly in the SOL/divertor) and with similar magnitudes. The impact on global confinement and the pedestal profiles of both of these species was also shown to be similar. Linear stability analysis of these points[5] also returned similar results, consistent with the peeling-ballooning theory. In order to differentiate between radiation and recycling induced changes in the fuelling profiles, neon can also be used as a radiator. A series of discharges were performed on AUG to compare the effects of neon and nitrogen.

Heating power was kept constant in these discharges at 13 MW (NBI + ECRH), as was the gas fuelling rate ($2.5 \times 10^{22} \text{e}^- \text{s}^{-1}$). The impurities were added with a small ramp and then a flat-top phase lasting 1.3 s to allow an equilibrium to be reached. An example timetrace for the neon seeded discharge is shown in figure 4. Two different steps of neon seeding were used, with more power radiated and a higher normalised beta reached during the phase with more neon seeding. A second discharge with higher levels was also attempted, but this disrupted due to impurity accumulation. A typical feature of the neon discharges is a higher ratio of main chamber to divertor radiation compared with nitrogen seeding. Overall, the divertor could not be

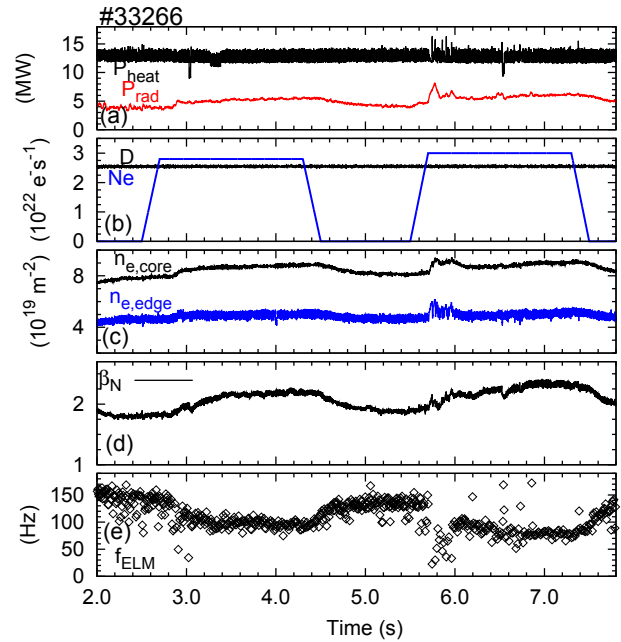


Figure 4: Time traces of (a) heating (black) and radiated (red) power, (b) fuelling waveforms for deuterium (black) and neon ($\times 10$, blue), (c) core (black) and edge (blue) line integrated densities, (d) normalised global beta and (e) ELM frequency for discharge #33266.

cooled as much with neon before a strong influx of tungsten occurred, resulting in the collapse of the discharge. It is thought that the tungsten influx results from higher divertor sputtering compounded by the lower ELM frequency associated with neon and its main chamber radiation.

Profile analysis of both the nitrogen and neon discharges was carried out, followed by detailed linear stability analysis to determine the applicability of the peeling-ballooning model to these scenarios. For the analysis, a reference phase (shown in red in the following figures), a neon seeded phase (shown in blue) and a nitrogen seeded phase from a separate discharge (shown in green) with similar total radiated power were analysed. Profiles of (a) electron temperature and (b) density as well as (c) the total real space pressure gradient are shown in figure 5. One striking difference between the nitrogen and neon seeded data are the responses of the profiles. Nitrogen seeding, as already shown[5], typically increases the temperature profile with no effect on the density profile other than the inward shift. However, in the case of neon seeding, the density pedestal top is also increased. This has been observed in many discharges with neon seeding and confinement improvement and therefore seems to be a general feature of neon seeding linked with confinement improvement. The mechanism by which this takes place (additional core fuelling by neon or a change of the recycling and fuelling sources) is currently under investigation.

The equilibria were produced using the measured pressure profiles and magnetic data using the CLISTE code[22, 23], which self consistently determines the edge current density. The resulting α profiles are shown in figure 6(a). In the neon case, the maximum α value has not changed. Instead, the gradient region has broadened, leading to the higher pedestal top pressure observed in the experiment. In the nitrogen seeded case, the peak α value has increased slightly, but the broadened gradient region is still the main feature and leads to the higher pedestal top value. These base equilibria (two from each discharge, one reference and one seeded) were then used as input for the HELENA fixed boundary equilibrium solver[24] and the WPCD j-alpha manipulator. A grid of modified equilibria for each time-point was then created and a range of mode numbers ($1 < n < 70$) were analysed using the MISHKA-fast[25] code. The stability boundaries in j- α space were then determined and are shown in figure 6(b).

In the neon seeded case, neither the measured operational point nor the calculated stability boundary change with impurity seeding. Instead, as has already been shown for a separate nitrogen seeded case[20], the gradient region has become wider, allowing a higher pedestal

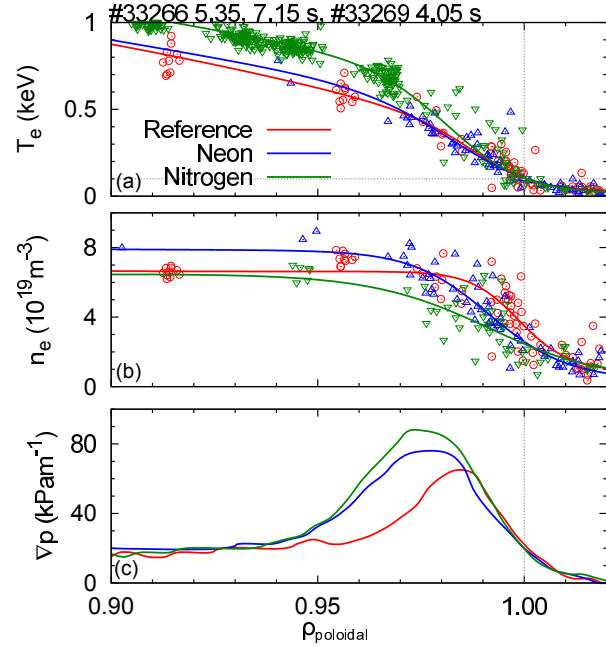


Figure 5: Profiles of (a) electron temperature (b) electron density and (c) the total pressure gradient for reference (red) neon seeded (blue) and nitrogen seeded (green) phases in two discharges (#33266, reference and neon and #33269, nitrogen).

top at the same critical pressure gradient. This can be understood since a main component of α is the q profile (a simple definition of α is $\alpha = -2 \times \frac{Rq^2}{B^2} \frac{dp}{dr}$); since there is a factor of q^2 included, a small shift of the gradient radially inwards leads to a much higher real space pressure gradient for the same α_{\max} , as observed in the experiment. In the nitrogen seeded case, consistent with the slightly higher measured α_{\max} , the stability boundary has moved to higher α . This small change is within the uncertainties (the error bars plotted indicate a 15% uncertainty in the pressure gradient and current density), so no definitive statement can be made.

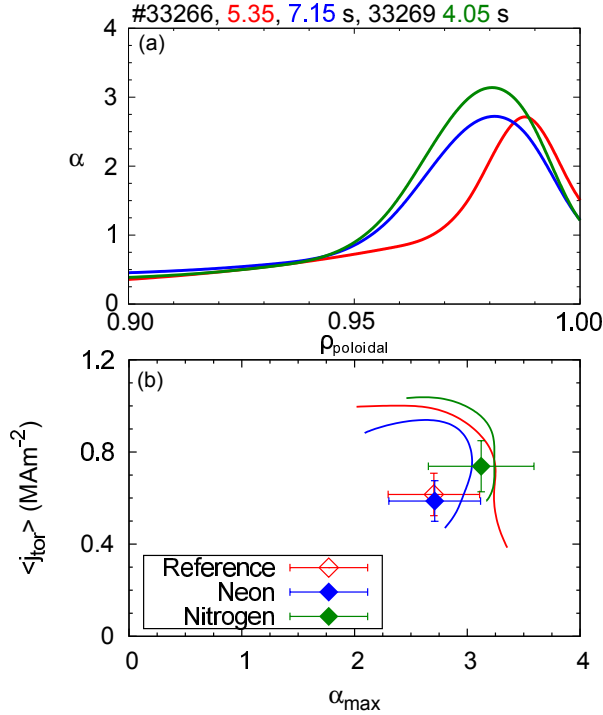


Figure 6: (a) Profile of α for reference (red), neon seeded (blue) and nitrogen seeded (green) time windows. (b) Stability diagram for the same phases.

file, based on experiments performed in a series of low triangularity discharges in AUG corresponds to a $\Delta\rho_{\text{poloidal}}$ of 0.01, or 5 mm in real space. Predictive pedestal simulations have previously shown[20] that this shift causes a decrease of the pedestal top pressure by 25%. This value agrees well with what is observed in the experiments.

By reducing the density in the HFSHD via impurity seeding (i.e. by radiating away the power required to ionise the neutrals near the inner divertor entrance) the density pedestal shifts radially inwards. This inward shift then allows the pedestal top pressure to increase to the values attained prior to the occurrence of the HFSHD. This has been tested extensively with nitrogen seeding[5] and a comparison with neon seeding has been presented in this paper. Since the mechanism is independent of the seeding impurity used, it is a promising method to mitigate any deleterious effects of excessive gas fuelling which is regularly used for ELM pacing and heat-load mitigation in metal-walled devices.

One difference between the two seeding species presented in this paper is that nitrogen typically increases the pedestal top temperature while neon acts on both temperature and density

A general conclusion, both from the analysis shown here and in previous studies[5, 15, 20], appears to be that impurity seeding reduces the HFSHD. This reduction then changes how the density pedestal is formed, resulting in an effective inward shift of the profile. This inward shift then results in a similar peak α value and a wider pedestal, the combination of which is a higher pedestal top pressure. This has now been shown for three radiating species (nitrogen, neon, and carbon) at low and high triangularity and therefore seems to be a general feature resulting from the change in fuelling mechanisms in the AUG pedestal.

5 Conclusions

To summarise the findings of the paper; the HFSHD, acting on the density profile location, acts to reduce the attainable pedestal top pressure. The outward shift of the density pro-

channels, though predominantly increases the pedestal top density. It is currently not known if this is via its reduction of the ELM frequency, that it radiates (and hence fuels) inside the confined region, or if it somehow changes the main chamber recycling (which determines the pedestal top density[16]). Further experiments with neon and argon seeding are planned, focussing in particular on achieving a cold divertor with neon; this may help to increase the ELM frequency in a manner similar to nitrogen seeding and, hence, mitigate the impurity peaking issues suffered during several experiments with neon seeding. If an integrated scenario with neon seeding can be achieved, it is quite promising not only for future JET-ILW operation, but also for future devices such as ITER and DEMO. While both neon and nitrogen can remove the deleterious effects of a highly fuelled plasma, only nitrogen has so far been able to cool the divertor significantly while remaining in a stable operating regime.

Acknowledgements

This work has been carried out within the framework of the EUROfusion Consortium and has received funding from the Euratom research and training programme 2014-2018 under grant agreement No 633053. The views and opinions expressed herein do not necessarily reflect those of the European Commission.

References

- [1] C.D. Challis, et al. *Nuclear Fusion*, 55(5), may 2015.
- [2] J. Schweinzer, et al. *Nuclear Fusion*, 51(11), nov 2011.
- [3] M.N.A. Beurskens, et al. *Plasma Physics and Controlled Fusion*, 55(12), dec 2013.
- [4] C Giroud, et al. *Plasma Physics and Controlled Fusion*, 57(3), mar 2015.
- [5] M.G. Dunne, et al. *Submitted to Plasma Physics and Controlled Fusion*, 2016.
- [6] P.B. Snyder, et al. *Nuclear Fusion*, 51(10), oct 2011.
- [7] S. Saarelma, et al. *Physics of Plasmas*, 22(5), may 2015.
- [8] C.F. Maggi, et al. *Nuclear Fusion*, 55(11), sep 2015.
- [9] D.R. Hatch, et al. *Nuclear Fusion*, 55(6), 2015.
- [10] R. Maingi, et al. *Physical Review Letters*, 107(14), sep 2011.
- [11] T.H. Osborne, et al. *Nuclear Fusion*, 55(6), jun 2015.
- [12] E Stefanikova, et al. Effect of the relative shift between the electron density and temperature pedestal position on the pedestal stability in JET-ILW. In *43rd EPS Conference on Plasma Physics*, page O4.117, 2016.
- [13] M G Bell, et al. *Plasma Physics and Controlled Fusion*, 51(12), dec 2009.
- [14] S. Potzel, et al. *Nuclear Fusion*, 54(1), jan 2014.
- [15] S. Potzel, et al. *Journal of Nuclear Materials*, dec 2014.
- [16] F. Reimold, et al. *Submitted to Journal of Nuclear Materials*, 2016.
- [17] M.N.a. Beurskens, et al. *Nuclear Fusion*, 54(4), apr 2014.
- [18] A. Kallenbach, et al. *Plasma Physics and Controlled Fusion*, 55(12), dec 2013.
- [19] M.L. Reinke, et al. *Journal of Nuclear Materials*, 415(1), aug 2011.
- [20] M G Dunne, et al. *Plasma Physics and Controlled Fusion*, Accepted, 2016.
- [21] M Beurskens, et al. *Nuclear Fusion*, 56, 2016.
- [22] P.J. McCarthy. *Physics of Plasmas*, 6(9), 1999.
- [23] P.J. McCarthy. *Plasma Physics and Controlled Fusion*, 54(1), jan 2012.
- [24] GTA Huysmans, et al. Helena. In *Conference on computational plasma physics (CP90)*, page 371, 1991.
- [25] A B Mikhailovskii. *Plasma Physics and Controlled Fusion*, 40, 1998.